J. Fluid Mech. (2004), *vol.* 521, *pp.* 295–317.
DOI: 10.1017/S002211200400179X Printed in the United Kingdom

Time-dependent response of a floating viscoelastic plate to an impulsively started moving load

By K. WANG[1], R. J. HOSKING[2] AND F. MILINAZZO[3]†

[1]Department of Mathematics, James Cook University, Townsville, Qld 4811, Australia

[2]Department of Mathematics, Universiti Brunei Darussalam, Gadong BE1410, Brunei

[3]Department of Mathematics, University of Victoria, Victoria, BC, Canada

(Received 28 May 2004 and in revised form 20 August 2004)

This paper extends the Boltzmann hereditary delay integral approach previously used to predict the anelastic response of a floating flexible plate to a steadily moving load, to describe the evolution of the response when the load is impulsively started from rest. Asymptotic analysis demonstrates that the ultimate one-dimensional and two-dimensional deflections (due to a line load and a point load, respectively) are consistent with the results obtained from the earlier time-independent viscoelastic theory. Transients in the two-dimensional case decay much more rapidly than their counterparts in the one-dimensional case. Steady-state deflections are approached at all load speeds in the two-dimensional theory, including the critical load speed (coincident with the minimum phase speed of hybrid flexural–gravity waves) and the gravity wave speed.

1. Introduction

A major motivation for the study of a moving load on a flexible beam or plate has been its application to transport systems (rail tracks, roads or runways), originally in temperate lands and subsequently in cold regions, where, in particular, floating ice sheets may be exploited. The response of a floating ice sheet to a land-based vehicle or landing aircraft has been modelled remarkably successfully by linear theory, with the ice treated as a thin elastic plate and associated pressure variations in the underlying water (defined by the Bernoulli equation for incompressible irrotational flow) included by assuming non-cavitation at the plate boundary. However, to allow for the anelastic behaviour of an ice sheet subjected to a moving load, a two-parameter Boltzmann hereditary delay integral approach to include viscoelasticity in the plate equation was introduced. This produced a pronounced but finite response (in lieu of the infinite deflection predicted for an elastic plate) at the critical load speed, which is the lower bound for load speeds at which hybrid flexural–gravity waves are generated, coincident with their minimum phase speed c_{min}. The viscoelastic theory also predicts that the maximum deflection occurs behind the load and explains other observed phenomena, including the asymmetric (rather than symmetric) quasi-static response when the load speed is below the critical speed, the more severe attenuation of the shorter predominantly flexural waves appearing ahead of the load above the critical speed,

† Author to whom correspondence should be addressed. fmilinaz@math.uvic.ca

and why the two-dimensional wave pattern may appear 'swept back' to some extent. Except when contributions from larger wavenumbers become significant, explicit consideration of finite plate thickness confirmed the validity of the thin-plate assumption, and convenient far-field asymptotic theory may be used. In-plane stress on the plate and water stratification are examples of other aspects also discussed in detail by Squire *et al.* (1996).

The emphasis in this paper is on time-dependent theory for the response of a floating viscoelastic plate to a moving load, whereas all such work published to date assumes that the thin plate is elastic. Thus, Schulkes & Sneyd (1988) reviewed the pioneering time-dependent analysis of Kheysin (1971) for a floating elastic plate, and showed that linear theory for the one-dimensional response due to an impulsively started steadily moving line load predicts two load speeds at which the deflection continuously grows with time. The two singular load speeds identified were the gravity wave speed $\sqrt{gH}$ and the minimum phase speed c_{min} of the hybrid flexural–gravity waves. However, the linear time-dependent theory for the two-dimensional response of a floating elastic plate to either a point load or a uniformly distributed circular or rectangular load demonstrates that only one of these two load speeds is critical (Nugroho *et al.* 1999). Thus, the deflection at the load speed coincident with the minimum phase speed c_{min} of the hybrid flexural–gravity waves also continuously grows in the two-dimensional theory, albeit more slowly than in the one-dimensional theory, that is as $\ln t$ rather than as $t^{1/2}$, for time $t \to \infty$. Transients found by Schulkes & Sneyd (1988) in the various load speed regimes are all moderated by a factor $t^{-1/2}$ as $t \to \infty$ in the two-dimensional theory, so the resultant steady-state deflections are reached more quickly than in the one-dimensional theory. Further, this moderating factor also applies at the load speed $\sqrt{gH}$, so that the two-dimensional theory predicts that the deflection at this speed does not grow, but approaches a steady state, although rather more slowly than at other load speeds (the transient component at $\sqrt{gH}$ decays as $t^{-1/3}$ for $t \to \infty$, and not as t^{-1} for $t \to \infty$ as do transients at other load speeds). This confirmed a prior suggestion that the response might not grow at the load speed coincident with the gravity wave speed $\sqrt{gH}$, since in two dimensions energy can radiate away in directions other than in the line of motion of the load. It was also anticipated from the linear two-dimensional time-independent analysis for the response of a floating thin elastic plate to a moving load, and in particular the observation by Milinazzo, Shinbrot & Evans (1995) that the steady-state deflection due to a steadily moving uniform rectangular load is everywhere finite at the load speed $\sqrt{gH}$. Numerical computations for the two-dimensional response also produce deflection and stress amplifications, defined as the maximum deflection and stress at the critical speed relative to the respective values due to a stationary load, which appear to agree more closely with experiment.

As stated above, linear time-independent viscoelastic theory for both the one-dimensional and two-dimensional response (due to both a line and point load) not only accounts for some otherwise unexplained observations in experiments involving moving loads on ice plates, but also removes the singularity found in the time-independent linear elastic theory, i.e. viscoelasticity introduced via a Boltzmann hereditary delay integral approach renders a pronounced but finite steady-state deflection at the critical load speed c_{min} (Hosking, Sneyd & Waugh 1988). In this paper, we pursue this approach to examine the evolution of the response of a floating flexible viscoelastic plate to a moving load impulsively started from rest (as in the previous time-dependent elastic theory). The two-parameter approximation previously used to reflect instantaneous and delayed elastic behaviour is again adopted. In § 2,

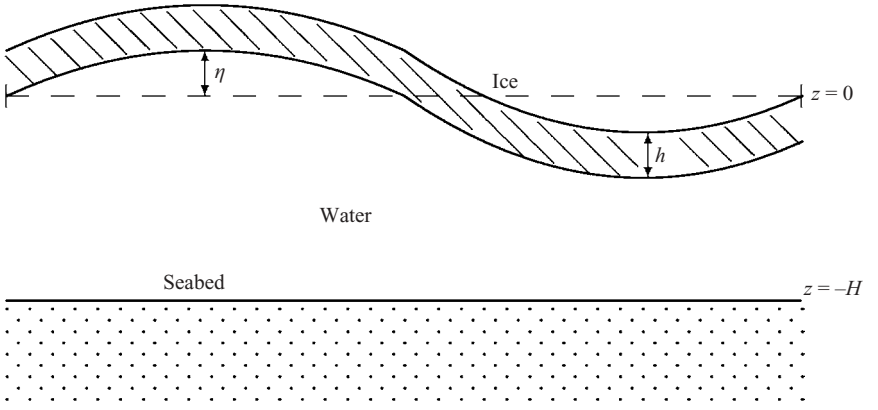

FIGURE 1. Diagram of a floating ice plate.

the fundamental mathematical model is re-stated and the time-dependent aspect is defined. In §§3 and 4, suitable renditions of the time-dependent viscoelastic Fourier integral are obtained for both the one-dimensional and two-dimensional deflections due to a line load and a point load, respectively, and these results are analysed asymptotically. The asymptotic analysis is complemented by numerical computation in §5, where wave patterns in the two-dimensional case are also presented. Concluding remarks are made in §6.

2. Mathematical model

The mathematical model describes a thin homogeneous plate of density ρ_0 floating on water of density ρ and depth H, where the undisturbed water surface is at $z=0$ and the underlying bed is at $z=-H$ (cf. figure 1). The plate is taken to be of infinite extent, in the usual sense that plate boundaries are assumed to have negligible influence. If $\eta(x, y, t)$ denotes the small vertical deflection due to a forcing function $f(x, y, t)$ representing the moving load, where x and y are the other Cartesian coordinates in the plane of the undisturbed horizontal surface and t is the time, then the hereditary delay differential equation for a thin viscoelastic plate is

$$D\nabla^4\left(\eta(x, y, t) - \int_0^\infty \Psi(\tau)\eta(x, y, t-\tau)\,\mathrm{d}\tau\right) + \rho_0 h\eta_{tt} = p - f(x, y, t), \qquad (1)$$

where $\Psi(t)$ is the viscoelastic memory function dependent upon the material properties of the plate, constant D is the effective flexural rigidity of the plate, h is the plate thickness, and p is the water pressure at $z=0$.

A sketch of the configuration in the context of a sea ice sheet is shown in figure 1. The detailed structure of ice, especially sea ice, is complex and its physical properties vary considerably with depth. However, the essential parameters in the viscoelastic form (1) of the otherwise classical differential equation for the deflection of a uniform plate may be suitably defined or interpreted. Moreover, a fully nonlinear viscoelastic constitutive relation for either freshwater ice or sea ice is unnecessary in the context of a moving load, when its speed is such that the model should represent instantaneous and delayed elastic behaviour, but not necessarily irrecoverable viscous creep. On the assumption that the memory of the ice fades with time, the memory function may be

represented as a finite sum of exponentials, i.e.

$$\Psi(t) = \sum_{j=0}^{n} A_j \exp(-\alpha_j t), \tag{2}$$

where the viscoelastic parameters A_j and α_j are real and positive. In common with the earlier time-independent viscoelastic theory of Hosking *et al.* (1988), the simplest possible representation is adopted here by setting $n=0$, when there are only two parameters involved, namely A_0, defining the magnitude of viscoelastic effects, and the reciprocal α_0 of the memory timescale. This simplest case nevertheless corresponds to a generalization of the memory function for the Maxwell viscoelastic model (where $0 < A_0 = \alpha_0$), and it is consistent with the so-called standard model of linear viscoelastic theory (visualized as a spring in series with a Voigt unit) provided $0 < A_0 \leqslant \alpha_0$. Further terms may be included in the finite sum to describe the response due to a slow or stationary load. However, this two-parameter anelastic theory for a thin plate has proved adequate to account for certain features observed in experiments involving moving loads on both freshwater and sea ice sheets (but not predicted in the theory for an elastic plate), as indicated above. Reference may again be made to Squire *et al.* (1996).

The water pressure at $z=0$ is defined by the linearized Bernoulli equation for incompressible irrotational flow

$$p = -\rho g \eta - \rho \left.\frac{\partial \phi}{\partial t}\right|_{z=0}, \tag{3}$$

where ϕ denotes the velocity potential satisfying the Laplace equation $\nabla^2 \phi = 0$ and the boundary condition $\partial\phi/\partial z|_{z=-H} = 0$ at the impenetrable bed. It is assumed here that there is neither significant water flow relative to the plate nor cavitation at the plate–water interface. No nonlinear term is included in the mathematical model, on the assumption that the amplitude of the plate deflection and the accompanying water displacement remains sufficiently small everywhere (but see later). However, it is difficult to envisage a suitable non-Eulerian alternative, given the typical quite irregular air–water interface, especially beneath a sea ice sheet. Finally, as previously observed, the plate acceleration term in (1) can be neglected for deflection wavelengths much larger than the plate thickness (Davys, Hosking & Sneyd 1985; Squire *et al.* 1996).

Substituting (3) into (1) and taking Fourier transforms such as

$$\hat{\eta}(k_1, k_2, \omega) = \frac{1}{(2\pi)^{3/2}} \iiint \eta(x, y, t) \exp(\mathrm{i}(k_1 x + k_2 y - \omega t))\, \mathrm{d}x\, \mathrm{d}y\, \mathrm{d}t \tag{4}$$

yields

$$\hat{\eta}(k_1, k_2, \omega) = \frac{-\hat{f}(k_1, k_2, \omega)}{Dk^4(1-\psi) + \rho g - \rho\omega^2 \coth(kH)/k}, \tag{5}$$

where $k^2 = k_1^2 + k_2^2$ and the viscoelasticity identified with

$$\psi(\omega) = \int_0^\infty \Psi(\tau)\, \mathrm{e}^{-\mathrm{i}\omega\tau}\, \mathrm{d}\tau \tag{6}$$

may affect all but the largest wavelengths ($k \simeq 0$). Corresponding to the simplest possible memory function involving only two viscoelastic parameters A_0 and α_0, (6)

rewritten as

$$\psi(\omega) = \frac{A_0}{\alpha_0 + \mathrm{i}\omega}$$

is deemed to suitably describe the viscoelastic behaviour of an ice sheet under the envisaged dynamic loading (provided $0 < A_0 \leqslant \alpha_0$) as outlined above.

Inversion of (4) yields the main point of departure for the analysis presented in this paper, i.e. the viscoelastic time-dependent Fourier integral for the deflection, which may be expressed as

$$\eta(x, y, t) = -\frac{\mathrm{i}}{(2\pi)^{3/2}\rho} \iiint \frac{g(k, \omega)\hat{f}(k_1, k_2, \omega)\exp(-\mathrm{i}(k_1 x + k_2 y - \omega t))}{W(k, \omega)}\, \mathrm{d}\omega\, \mathrm{d}k_1\, \mathrm{d}k_2. \tag{7}$$

Here, $g(k, \omega) = (\alpha_0 + \mathrm{i}\omega)k\tanh(kH)$ and $W(k, \omega) = \omega^3 + \mathrm{i}p\omega^2 + q\omega + \mathrm{i}r$, a cubic in ω for fixed k, where

$$p = -\alpha_0, \quad q = -(Dk^4 + \rho g)\frac{k}{\rho}\tanh(kH), \quad r = [(Dk^4 + \rho g)\alpha_0 - Dk^4 A_0]\frac{k}{\rho}\tanh(kH). \tag{8}$$

Both q and r are real functions even in k (and p is constant), so the three roots ω of the equation $W(k, \omega) = 0$ are even functions of k. For any given wavenumber $k \neq 0$, two of these are complex roots symmetric about the imaginary axis, and the third is pure imaginary, namely

$$\omega_{1,2} = \pm\frac{\sqrt{3}}{2}(A - B) + \mathrm{i}\left[\frac{\alpha_0}{3} - \tfrac{1}{2}(A + B)\right], \qquad \omega_3 = \mathrm{i}\left(\frac{\alpha_0}{3} + A + B\right), \tag{9}$$

where A and B are real even functions in k, dependent upon the viscoelastic parameters A_0 and α_0 (cf. the Appendix). In passing, it is notable that $A > B$ for $k \neq 0$, $\mathrm{Im}(\omega_{1,2}) > 0$ monotonically increases from zero at $k = 0$, and $\mathrm{Im}(\omega_3) > 0$ monotonically decreases from its maximum α_0 at $k = 0$.

If the viscoelastic parameter A_0 is set to zero, then

$$\frac{g(k, \omega)}{W(k, \omega)} = \frac{\mathrm{i}k\tanh(kH)}{\omega^2 + q}$$

and hence the Fourier integral in (7) reduces to the form in the elastic limit, where the quadratic equation $\omega^2 + q = 0$ is the familiar dispersion relation for hybrid flexural–gravity waves (Squire *et al.* 1996). Indeed, for small but finite viscoelastic parameter A_0, the related contributions in (9) are

$$\frac{\sqrt{3}}{2}(A - B) = |k|c(k) + O(A_0), \qquad A + B = \tfrac{2}{3}\alpha_0 + O(A_0), \tag{10}$$

where $c(k)$ denotes the flexural-gravity wave phase speed in the absence of viscoelasticity. Thus, in the elastic limit when $A_0 = 0$, the two roots $\omega_{1,2} = \pm|k|c(k)$ are real and the method of stationary phase may be invoked to evaluate the deflection asymptotically as time $t \to \infty$ (cf. Schulkes & Sneyd 1988; Nugroho *et al.* 1999).

In contrast, with the viscoelasticity included (i.e. when $A_0 \neq 0$) both of these two roots $\omega_{1,2}$ are complex and non-zero provided $k \neq 0$ as shown in (9), and the major contribution in the asymptotic analysis for $t \to \infty$ of each of the two related integrals comes from the neighbourhood of the endpoint $k = 0$. The integral corresponding to the additional imaginary root ω_3 is likewise assessed asymptotically, after the point at infinity ($k = \infty$) is first mapped to the origin ($k = 0$).

3. Line load

3.1. *The time-dependent deflection*

An impulsively started concentrated (y-independent) line load of weight F_0 subsequently travelling with uniform speed V in the positive x-direction is represented by the loading function $f(x,t)=F_0\delta(x-Vt)H(t)$, where δ denotes the Dirac delta function and $H(t)$ is the Heaviside unit step function. The Fourier transform of this loading function is (Wong 1989)

$$\hat{f}(k,\omega)=\frac{F_0}{2}\left[\delta(\omega-kV)+\frac{1}{\pi\mathrm{i}(\omega-kV)}\right],$$

so from (7) the deflection is

$$\eta(X,t)=-\frac{\mathrm{i}F_0}{4\pi\rho}\int\frac{g(k,kV)\exp(-\mathrm{i}kX)}{W(k,kV)}\,\mathrm{d}k - \frac{F_0}{4\pi^2\rho}\iint\frac{g(k,\omega)\exp(-\mathrm{i}[kX-(\omega-kV)t])}{W_L(\omega)}\,\mathrm{d}\omega\,\mathrm{d}k, \quad (11)$$

where the coordinate $X=x-Vt$ is relative to the moving load and the variable k has been suppressed in defining $W_L(\omega)=(\omega-kV)W(k,\omega)$.

Contour integration may be used to perform the integration with respect to ω in the second integral of (11). The poles for the contour integration correspond to the four roots of the quartic equation $W_L(\omega)=0$, namely $\omega_0=kV$ and the three roots defined in (9). For notational brevity, hereinafter let us write $\omega_{1,2}=\pm\lambda+\mathrm{i}\mu$ and $\omega_3=\mathrm{i}\nu$ where

$$\lambda=\frac{\sqrt{3}}{2}(A-B),\qquad \mu=\tfrac{1}{3}\alpha_0-\tfrac{1}{2}(A+B),\qquad \nu=\tfrac{1}{3}\alpha_0+A+B. \quad (12)$$

For $k\neq 0$, all four roots are distinct. Three of the four roots merge into the origin (i.e. $\omega_{0,1,2}=0$) at $k=0$, but the viscoelastic plate term in (5) vanishes in this infinite wavelength limit, and the degeneracy is avoided by implicitly excluding the point $k=0$ (of measure zero) from any range of integration in the following analysis.

By introducing partial fractions, the second integral in (11) may be partitioned as

$$\frac{F_0}{4\pi^2\rho}\sum_{j=0}^{3}\int_{-\infty}^{\infty}\int_{-\infty}^{\infty}\frac{g(k,\omega)\exp(-\mathrm{i}[kX-(\omega-kV)t])}{W_L'(\omega_j)(\omega-\omega_j)}\,\mathrm{d}\omega\,\mathrm{d}k,$$

where the derivative W_L' (with respect to ω) evaluated at ω_j conveniently represents the product of three factors $(\omega_j-\omega_k)$, $k\neq j$. Then, integrating this partitioned result with respect to ω using the Cauchy residue theorem and absorbing the first integral in (11) yields the deflection in the form

$$\eta(X,t)=\frac{F_0}{2\pi\rho}(I_0+I_1+I_2+I_3), \quad (13)$$

where

$$I_j(X,t)=-\mathrm{i}\int_{-\infty}^{\infty}\frac{g(k,\omega_j)\exp(-\mathrm{i}[kX-(\omega_j-kV)t])}{W_L'(\omega_j)}\,\mathrm{d}k. \quad (14)$$

The time-independent contribution obtained from I_0 is identical to the steady-state viscoelastic result (3.1) of Hosking *et al.* (1988) for a line load, and the time-dependent behaviour resides in the contribution from the remaining integrals I_1, I_2 and I_3.

3.2. *Asymptotic analysis*

In the elastic limit $A_0 \to 0$, from (10) and (12) we have $\lambda = |k|c(k)$, $\mu = 0$ and $\nu = \alpha_0$ so that $I_3 \to 0$ and

$$I_1 + I_2 \to \int_0^\infty \frac{\tanh(kH)}{c(k)} \left\{ \frac{\cos(kX - \psi_1 t)}{\psi_1(k)} + \frac{\cos(kX + \psi_2 t)}{\psi_2(k)} \right\} \mathrm{d}k, \tag{15}$$

where $\psi_1(t) = k(c - V)$ and $\psi_2(t) = k(c + V)$ are the phase functions (cf. Schulkes & Sneyd 1988; Squire *et al.* 1996). In this elastic limit, let us recall that the dominant asymptotic contributions as $t \to \infty$, arise from the neighbourhood of points of stationary phase, where $\psi_1'(k) = 0$, i.e. at values of k where the group speed of the hybrid flexural–gravity waves generated coincides with the sufficiently high load speed ($c_g(k) = V$).

As mentioned previously, however, with viscoelasticity included, the asymptotic analysis is different and invokes properties of the three roots $\{\omega_j(k), j = 1, 2, 3\}$ discussed in the Appendix. Thus, in all of our asymptotic calculations as $t \to \infty$ below, the focus is on interval endpoints at which the integrands peak, when it is pertinent to recall that: (*a*) the imaginary part $\mu = \alpha_0/3 - (A + B)/2$ of $\omega_{1,2}$, which is the real exponential coefficient in the integrands of I_1 and I_2, monotonically increases from its minimum (namely $\mu = 0$) at $k = 0$; whereas (*b*) the real exponential coefficient $\nu = \alpha_0/3 + A + B$ in the integrand of I_3 corresponding to ω_3 attains its maximum (namely $\nu = \alpha_0$) at $k = 0$ and monotonically decreases with k, so we first map the point at infinity to the origin to evaluate I_3 asymptotically. Moreover, rather than asymptotically estimating integrals for large time t directly, our calculations are simplified by estimating the derivatives of such integrals with respect to t instead, from which the asymptotic behaviour of the original integrals can be deduced (see also Olver 1974; Nugroho *et al.* 1999).

Recalling (12), the time derivatives of the integrals $I_j(X, t)$ for $j = 1, 2, 3$ in (14) are

$$\begin{aligned} I_{1,t}(X, t) &= \int_{-\infty}^{\infty} \frac{g(k, \omega_1) \exp(-\mathrm{i}[kX - (\omega_1 - kV)t])}{(\omega_1 - \omega_2)(\omega_1 - \omega_3)} \mathrm{d}k \\ &= \int_{-\infty}^{\infty} k \tanh(kH) \frac{(\alpha_0 - \mu + \mathrm{i}\lambda) \exp(-\mu t) \exp(-\mathrm{i}[kX - (\lambda - kV)t])}{2\lambda[\lambda + \mathrm{i}(\mu - \nu)]} \mathrm{d}k \end{aligned}$$

and

$$\begin{aligned} I_{2,t}(X, t) &= \int_{-\infty}^{\infty} \frac{g(k, \omega_2) \exp(-\mathrm{i}[kX - (\omega_2 - kV)]t)}{(\omega_2 - \omega_1)(\omega_2 - \omega_3)} \mathrm{d}k \\ &= \int_{-\infty}^{\infty} k \tanh(kH) \frac{(\alpha_0 - \mu - \mathrm{i}\lambda) \exp(-\mu t) \exp(-\mathrm{i}[kX + (\lambda + kV)t])}{2\lambda[\lambda - \mathrm{i}(\mu - \nu)]} \mathrm{d}k, \end{aligned} \tag{16}$$

so that

$$\begin{aligned} I_{1,t}(X, t) + I_{2,t}(X, t) = \int_0^\infty \mathrm{e}^{-\mu t} \{ & A_1(k)[\sin(kX - \Psi_1 t) - \sin(kX + \Psi_2 t)] \\ & + A_2(k)[\cos(kX - \Psi_1 t) + \cos(kX + \Psi_2 t)] \} \mathrm{d}k. \end{aligned} \tag{17}$$

Here, the maximum amplitude functions are

$$A_1(k) = k \tanh(kH) \frac{\lambda^2 + (\mu - \alpha_0)(\mu - \nu)}{\lambda[\lambda^2 + (\mu - \nu)^2]}, \quad A_2(k) = k \tanh(kH) \frac{\alpha_0 - \nu}{\lambda^2 + (\mu - \nu)^2}, \tag{18}$$

and $\Psi_1(k) = \lambda - kV$ and $\Psi_2(k) = \lambda + kV$ are the phase functions including viscoelasticity.

The first integral in (17) resembles the time derivative of the integral in the elastic limit given in (15), when $\nu = \alpha_0$ and the second integral in (17) vanishes, but the additional $\exp(-\mu t)$ factor introduced by the viscoelasticity plays an essential role in the analysis here. Thus, the asymptotic evaluation of the integrals in (17) as $t \to \infty$ follows from the behaviour of the amplitudes and phase functions in the neighbourhood of $k = 0$, where the exponential coefficient μ attains its minimum (cf. Olver 1974, chap. 4, § 6). As was foreshadowed following (12), the point $k = 0$ at which $\mu = 0$ is excluded from the range of integration by requiring $k \geqslant \epsilon > 0$, such that the minimum of μ occurring near $k = 0$ is small but positive and hence the integrands in (17) decay exponentially with time. Nevertheless, for asymptotic purposes, the decay factor is negligible sufficiently close to $k = 0$ (as $\epsilon \to 0$), where the leading terms in the Taylor series for the amplitude and phase functions are

$$A_1(k) \simeq k\sqrt{\frac{H}{g}}, \qquad A_2(k) = O(A_0 D k^8), \qquad \Psi_{1,2}(k) \simeq k[c(k) \mp V],$$

where $c(k) = \sqrt{gH}(1 - k^2H^2/6 + \cdots)$. Consequently, although one amplitude function and both phase functions are independent of viscoelasticity to leading order near $k = 0$, when $V \neq \sqrt{gH}$ such that $\Psi_{1,2} = O(k)$, we have (*a*) the first integral in (17) with amplitude function $A_1(k)$ is $O(t^{-2})$ as $t \to \infty$; and (*b*) the second integral in (17) with amplitude function $A_2(k)$ is not only proportional to the viscoelastic parameter A_0, but also asymptotically smaller as $t \to \infty$. Thus, the $\exp(-\mu t)$ factor introduced by the viscoelasticity then ensures that the $I_1 + I_2$ contribution to the deflection in (13) is transient $O(t^{-1})$ as $t \to \infty$ – even at the critical load speed $V = c_{min}$, where the time-dependent elastic theory predicts that the deflection does not approach a steady state. On the other hand, when $V = \sqrt{gH}$ so that the phase function $\Psi_1 \simeq k^3H^3/6$ to leading order, this asymptotic analysis reproduces the elastic growth rate $O(t^{1/3})$ as $t \to \infty$ for the one-dimensional response to a line load (Schulkes & Sneyd 1988; Squire *et al.* 1996).

The time derivative of the integral $I_3(X, t)$, arising due to the additional imaginary root ω_3 introduced by the viscoelasticity (cf. (9)), is

$$\begin{aligned} I_{3,t}(x,t) &= \int_{-\infty}^{\infty} \frac{g(k,\omega_3)\exp(-\mathrm{i}[kX - (\omega_3 - kV)t])}{(\omega_3 - \omega_1)(\omega_3 - \omega_2)}\,\mathrm{d}k \\ &= -\int_{-\infty}^{\infty} k\tanh(kH)\frac{(\alpha_0 - \nu)\exp(-\nu t)\exp(-\mathrm{i}k(X + Vt))}{\lambda^2 + (\mu - \nu)^2}\,\mathrm{d}k \\ &= -2\int_0^{\infty} A_2(k)\exp(-\nu t)\cos[k(X + Vt)]\,\mathrm{d}k. \end{aligned} \tag{19}$$

Let us recall that $\nu \equiv \mathrm{Im}(\omega_3) > 0$ decreases monotonically as k increases, and the amplitude function $A_2(k)$ here is defined in (18) above. After mapping the point at infinity ($k = \infty$, where ν attains its minimum) to the origin ($k = 0$), we have $\nu = \alpha_0 - A_0 + O(k^4)$ and $A_2(k) = O(k^5)$, so that $I_{3,t}(X, t) = O(A_0 t^{-3/2}\exp[-(\alpha_0 - A_0)t])$. In § 2, we noted the requirement that $A_0 \leqslant \alpha_0$, hence for $t \to \infty$ the integral in (19) is proportional to the viscoelastic coefficient A_0, and decays either exponentially when $A_0 < \alpha_0$ or $O(t^{-3/2})$ when $A_0 = \alpha_0$. Thus, the I_3 contribution to the deflection in (13) is also transient, decaying either exponentially when $A_0 < \alpha_0$ or $O(t^{-1/2})$ when $A_0 = \alpha_0$, as $t \to \infty$.

4. Point load

4.1. *The time-dependent deflection*

For an impulsively started localized (point) load of weight F_0 subsequently travelling with uniform speed V in the positive x-direction, the loading function is $f(x, y, t) = F_0\delta(x - Vt)\delta(y)H(t)$, with Fourier transform (Wong 1989)

$$\hat{f}(k_1, k_2, \omega) = \frac{F_0}{\sqrt{8\pi}}\left[\delta(\omega - kV) + \frac{1}{\pi\mathrm{i}(\omega - k_1V)}\right].$$

Thus in this case, on again introducing the coordinate $X = x - Vt$ relative to the moving reference frame of the load, from (7) the deflection is

$$\eta(X, y, t) = -\frac{F_0}{8\pi^2\rho}\iint \frac{g(k, kV)\exp(-\mathrm{i}(k_1X + k_2y))}{W(k, k_1V)}\,\mathrm{d}k_1\,\mathrm{d}k_2 - \frac{F_0}{8\pi^3\rho}\iiint \frac{g(k, \omega)\exp(-\mathrm{i}[k_1X + k_2y - (\omega - k_1V)t])}{W_P(\omega)}\,\mathrm{d}\omega\,\mathrm{d}k_1\,\mathrm{d}k_2, \quad (20)$$

where $k^2 = k_1^2 + k_2^2$ and $W_P(\omega) \equiv (\omega - k_1V)W(\omega)$.

Our analysis here is at first quite similar to that given for the line load in the previous section. Thus, except at $k = 0$, the quartic $W_P(\omega)$ has four distinct roots, namely the suitably modified $\omega_0 = k_1V$, and precisely the same three roots $\omega_{1,2,3}$ as defined via (12). Hence, implicitly excluding the point at $k = 0$, the second integral in (20) may be partitioned as

$$\frac{F_0}{8\pi^3\rho}\sum_{j=0}^{3}\iiint \frac{g(k, \omega)\exp(-\mathrm{i}[k_1X + k_2y - (\omega - k_1V)t])}{W_P'(\omega_j)(\omega - \omega_j)}\,\mathrm{d}\omega\,\mathrm{d}k_1\,\mathrm{d}k_2,$$

where the prime on $W_P(\omega)$ again denotes differentiation with respect to variable ω. Then, integrating with respect to ω via the Cauchy residue theorem, from (20) the deflection in a form analogous to (13) is

$$\eta(X, y, t) = \frac{F_0}{4\pi^2\rho}(I_0 + I_1 + I_2 + I_3), \quad (21)$$

but now involving double integrals

$$I_j(X, y, t) = -\mathrm{i}\int_{-\infty}^{\infty}\int_{-\infty}^{\infty} \frac{g(k, \omega_j)\exp(-\mathrm{i}[k_1X + k_2y - (\omega_j - k_1V)t])}{W_P'(\omega_j)}\,\mathrm{d}k_1\,\mathrm{d}k_2. \quad (22)$$

The time-independent contribution obtained from the integral I_0 here is identical to the steady-state viscoelastic result (4.2) of Hosking *et al.* (1988) for a point load, and the time-dependent behaviour again resides in the contribution from the remaining integrals denoted by I_1, I_2 and I_3.

4.2. *Asymptotic analysis*

To analyse the time-dependence defined by the three double integrals $I_{1,2,3}$ in (22), it is again convenient to consider their time derivatives, but now also introduce polar coordinates (cf. Nugroho *et al.* 1999). Thus, under the coordinate transformation $X = r\cos\xi$, $y = r\sin\xi$, $k_1 = k\cos\theta$ and $k_2 = k\sin\theta$, it follows, for example, that

$$I_{1,t}(r, \xi, t) = \int_0^{\infty}\int_{-\pi}^{\pi} \frac{kg(k, \omega_1)\exp(-\mathrm{i}[kr\cos(\theta - \xi) - (\omega_1 - kV\cos\theta)t])}{(\omega_1 - \omega_2)(\omega_1 - \omega_3)}\,\mathrm{d}\theta\,\mathrm{d}k, \quad (23)$$

where it is notable that the roots $\omega_{1,2,3}$ are functions of k but not θ. Integrating with respect to θ therefore yields

$$I_{1,t}(r,\xi,t)=2\pi\int_0^\infty \frac{kg(k,\omega_1)J_0(kQ)\exp(\mathrm{i}\omega_1 t)}{(\omega_1-\omega_2)(\omega_1-\omega_3)}\,\mathrm{d}k, \tag{24}$$

where J_0 is the Bessel function of zero order and $Q=\sqrt{(r\cos\xi+Vt)^2+r^2\sin^2\xi}$. As time $t\to\infty$, the inequality $|r|\ll Vt$ is satisfied in an ever expanding region surrounding the localized (point) load at $r=0$, so that in the neighbourhood of the load $J_0(kQ)\simeq(2/\pi kVt)^{1/2}\cos(kVt-\pi/4)$.

The expression for the sum $I_{1,t}(r,\xi,t)+I_{2,t}(r,\xi,t)$ analogous to (17) is

$$\begin{aligned}\int_0^\infty\int_{-\pi/2}^{\pi/2} k\,\mathrm{e}^{-\mu t}\{&A_1(k)(\sin[kr\cos(\theta-\xi)-(\lambda-kV\cos\theta)t]-\sin[kr\cos(\theta-\xi)\\&+(\lambda+kV\cos\theta)t])+A_2(k)(\cos[kr\cos(\theta-\xi)-(\lambda-kV\cos\theta)t]\\&+\cos[kr\cos(\theta-\xi)+(\lambda+kV\cos\theta)t])\}\,\mathrm{d}\theta\,\mathrm{d}k,\end{aligned}$$

where the amplitudes $A_1(k)$ and $A_2(k)$ are the same as for the line load, i.e. as defined in (18). Integration with respect to θ then produces

$$I_{1,t}(r,\xi,t)+I_{2,t}(r,\xi,t)=2\pi\int_0^\infty k\,\mathrm{e}^{-\mu t}J_0(kQ)[-A_1(k)\sin(\lambda t)+A_2(k)\cos(\lambda t)]\,\mathrm{d}k. \tag{25}$$

In the elastic limit, (25) and the previous expression reduce to the time derivative of each of the corresponding expressions in equation (3.8) of Nugroho *et al.* (1999).

The anelastic response as $t\to\infty$ may be assessed from (25) by first invoking $J_0(kQ)\simeq(2/\pi kVt)^{1/2}\cos(kVt-\pi/4)$, so that we may consider the asymptotic behaviour of the result

$$\begin{aligned}&t^{-1/2}\int_0^\infty k^{1/2}\,\mathrm{e}^{-\mu t}\left[-A_1(k)\cos\left(kVt-\tfrac{1}{4}\pi\right)\sin(\lambda t)+A_2(k)\cos\left(kVt-\tfrac{1}{4}\pi\right)\cos(\lambda t)\right]\mathrm{d}k\\&\quad=t^{-1/2}\int_0^\infty k^{1/2}\,\mathrm{e}^{-\mu t}\left\{-A_1(k)\left[\sin\left(\Psi_1 t+\tfrac{1}{4}\pi\right)+\sin\left(\Psi_2 t-\tfrac{1}{4}\pi\right)\right]\right.\\&\qquad\left.+A_2(k)\left[\cos\left(\Psi_1 t+\tfrac{1}{4}\pi\right)+\cos\left(\Psi_2 t-\tfrac{1}{4}\pi\right)\right]\right\}\mathrm{d}k,\end{aligned} \tag{26}$$

where as before $\Psi_1(k)=\lambda-kV$ and $\Psi_2(k)=\lambda+kV$ are the phase functions with viscoelasticity. Comparison may be made with the integrals in (17) when $X=0$, to encapsulate just how the two-dimensional response (due to a point load) essentially differs from the one-dimensional response (due to a line load). Thus, apart from phase shifts, there is an additional $t^{-1/2}$ factor outside the integral (26), and an additional $k^{1/2}$ factor inside this integral. The asymptotic analysis of this integral must of course allow for the additional $k^{1/2}$ factor, but otherwise it is quite similar to the analysis in the previous section. Hence, when the additional $t^{-1/2}$ factor is also included, it follows that the I_1+I_2 contribution to the deflection in (21) is transient $O(t^{-2})$ as $t\to\infty$, even at the critical load speed $V=c_{min}$ – and indeed at all load speeds except the gravity wave speed $\sqrt{gH}$, when the elastic decay rate $O(t^{-1/3})$ as $t\to\infty$ found by Nugroho *et al.* (1999) is recovered.

The contribution from the additional imaginary root ω_3 is again transient. This follows from the time derivative

$$I_{3,t}(r, \xi, t) = 2\pi \int_0^\infty \frac{kg(k, \omega_3) J_0(kQ) \exp(i\omega_3 t)}{(\omega_3 - \omega_1)(\omega_3 - \omega_2)} \, dk \tag{27}$$

analogous to (24), and hence the asymptotic behaviour as $t \to \infty$ of

$$t^{-1/2} \int_0^\infty k^{1/2} e^{-\nu t} A_2(k) \cos(kVt - \pi/4) \, dk$$

analogous to the dominant component of (26), where $A_2(k)$ is again defined in (18). Thus, mapping the point at infinity ($k = \infty$) to the origin ($k = 0$) once more, it emerges that the I_3 contribution in (21) is proportional to A_0 and decays either exponentially when $A_0 < \alpha_0$ or $O(t^{-15/8})$ when $A_0 = \alpha_0$, as $t \to \infty$.

5. Numerical computation

To complement the asymptotic results obtained in the preceding two sections, the evolution of the deflection may be determined numerically from the complete time-dependent expressions, namely (13) and (14) for the line load, or (21) and (22) for the point load. We adopted the physical parameters $D = 7.324 \times 10^9$ N m^{-2}, $\rho = 10^3$ kg m^{-3}, $h = 2.5$ m and $H = 350$ m, as in previous calculations for a floating ice plate in the Antarctic (cf. Davys *et al.* 1985; Squire *et al.* 1996); and also the viscoelastic parameters $A_0 = \alpha_0 = 0.1$ s^{-1} as in Hosking *et al.* (1988), unless otherwise indicated.

5.1. *Line load*

For convenience, the constant factor $F_0/(2\pi\rho)$ in (13) was ignored, since the time variation and the relative magnitude of the deflections (rather than their actual magnitudes) are of most interest. The integrals in (14) were computed by fast Fourier transform, with grid sizes corresponding to both 4096 and 8192 points to provide an implicit check on accuracy. Time development of the deflection is shown in figures 2 to 4 for the respective load speeds $V = 18$ m s$^{-1} < c_{min}$(subcritical), $V = c_{min} = 22.5$ m s^{-1}(critical), and $c_{min} < V = 30$ m s$^{-1} < \sqrt{gH}$(supercritical). As anticipated from the previous time-independent viscoelastic theory (Hosking *et al.* 1988), the maximum deflection lags behind the load (here shown moving from right to left), and it now appears that this phenomenon occurs quite soon after a load begins to move. The time development of the deflection at the higher gravity wave speed $V = \sqrt{gH} = 58.6$ m s^{-2}, and at an even higher representative load speed $\sqrt{gH} < V = 70$ m s^{-2} when there are no trailing waves, are shown in figures 5 and 6, respectively. As is evident in these figures, the largest maximum deflection at any time t occurs at the critical speed $V = c_{min}$. The relatively small maximum deflections at the higher load speeds shown in figures 5 and 6 are comparable to the leading flexural wave amplitudes elsewhere.

Except at $V = \sqrt{gH}$, the deflections approached a steady state, and the typical time required was about a minute. At the load speed $V = \sqrt{gH}$, the only load speed at which the viscoelastic deflection continued to grow, the maximum response was not comparable with others until at least ten minutes had elapsed (cf. figure 7), and even then, it remained almost an order of magnitude smaller than the maximum deflection at the critical speed $V = c_{min}$. The time required to approach a steady state (at any load speed other than $\sqrt{gH}$) was found to be much the same for different viscoelastic

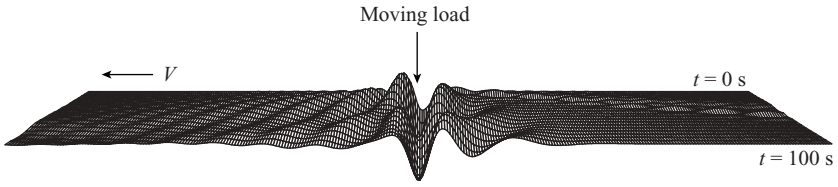

FIGURE 2. The time development of the deflection for a line load moving at the representative subcritical speed $V = 18\,\mathrm{m\,s^{-1}} < c_{min}$. The parameters are $A_0 = \alpha_0 = 0.1$; $D = 7.324 \times 10^9\,\mathrm{N\,m^{-2}}$; $\rho = 1000\,\mathrm{kg\,m^{-3}}$; $g = 9.8\,\mathrm{m\,s^{-2}}$; $H = 350\,\mathrm{m}$.

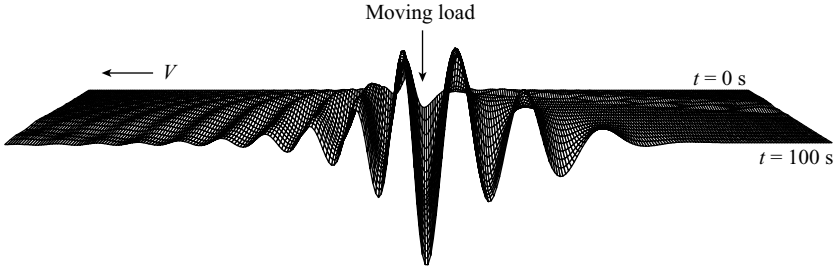

FIGURE 3. The time development of the wave system for a line load moving at the critical speed $V = 22.5\,\mathrm{m\,s^{-1}}$. The parameters are as in figure 2. The maximum value is approximately 4×10^{-5} (m).

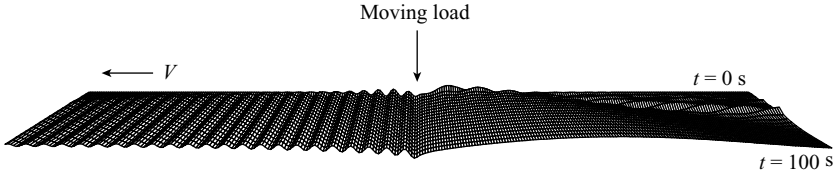

FIGURE 4. The time development of the wave system for a line load moving at the representative supercritical speed $c_{min} < V = 30\,\mathrm{m\,s^{-1}} < \sqrt{gH}$. The parameters are as in figure 2. The maximum value is approximately 1.5×10^{-5} (m).

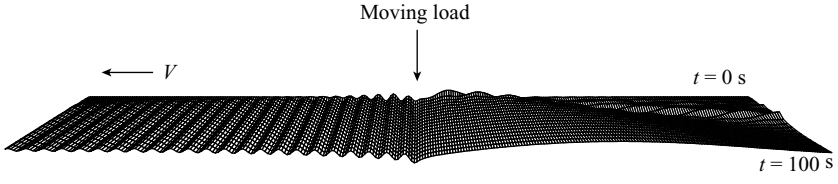

FIGURE 5. The time development of the wave system for a line load moving at the gravity wave speed $V = \sqrt{gH} = 58.6\,\mathrm{m\,s^{-1}}$. The parameters are as in figure 2.

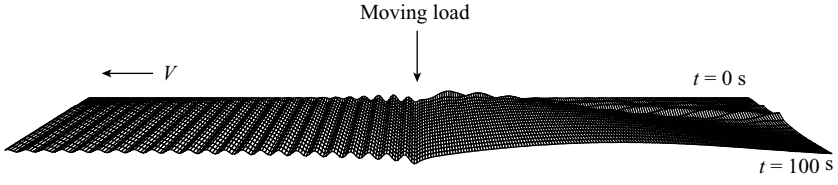

FIGURE 6. The time development of the wave system for a line load moving at the rather high speed $\sqrt{gH} < V = 70\,\mathrm{m\,s^{-1}}$. The parameters are as in figure 2. The maximum value is approximately 2×10^{-6} (m).

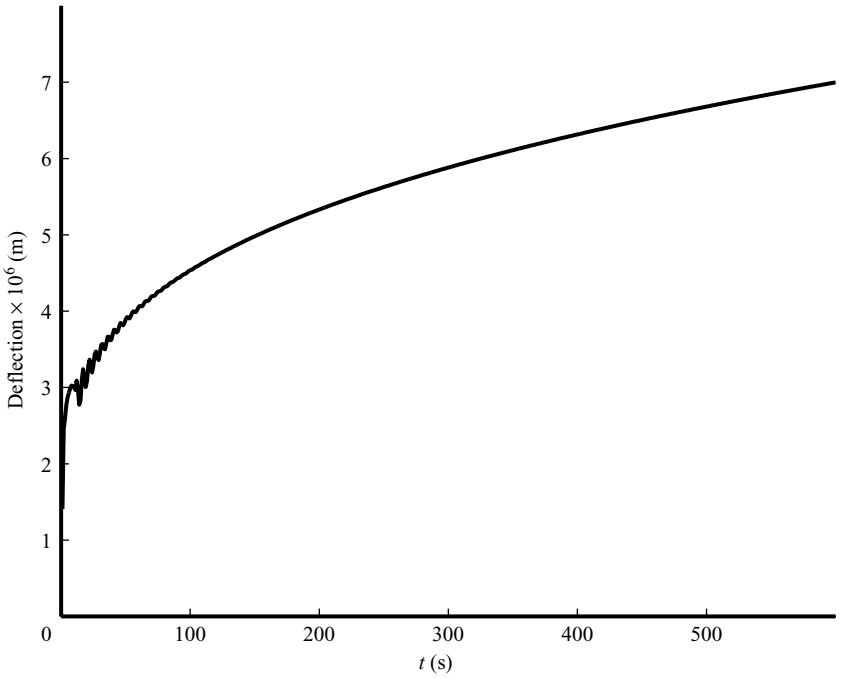

FIGURE 7. The maximum deflection versus time for a line load moving at the gravity wave speed $V = \sqrt{gH} = 58.6\,\mathrm{m\,s^{-1}}$.

parameters, but the eventual maximum deflection varied as the time-independent viscoelastic theory predicts – including the result that the pronounced maximum deflection at the critical load speed $V = c_{min}$ is moderated most of all (cf. figure 9 in Hosking *et al.* 1988 in particular). Thus, while the maximum deflection at $V = c_{min}$ in the elastic limit ($A_0 = 0$) continually tended higher with time as the elastic theory of Schulkes & Sneyd (1988) predicts, it always approached a steady-state value which decreased most as the viscoelastic parameter $A_0 \leqslant \alpha_0 = 0.1$ was increased from zero.

5.2. *Point load*

Two-dimensional steady-state wave patterns produced at various load speeds were first derived by Davys *et al.* (1985), from far-field asymptotic theory for a steadily moving point load on a floating elastic plate. Wave surface plots for a distributed uniform (rectangular) load were given by Milinazzo *et al.* (1995), with less reliance on the far-field approximation. Bukatov & Zharkov (1989) avoided the far-field assumption altogether and included time dependence, and obtained similar deflection fields (cf. also Squire *et al.* 1996).

Numerical computation for a point load from equations (21) and (22) yielded an ultimate steady-state response at every load speed considered, including $V = \sqrt{gH}$. Moreover, a steady state was approached quite quickly for each of the regimes represented in figures 2 to 4. An example of the typical rapid time development of the wave pattern produced is illustrated in figure 8, for a representative supercritical load speed $c_{min} < V = 40\,\mathrm{m\,s^{-1}} < \sqrt{gH}$. Figure 9 shows the viscoelastic wave pattern contours computed for the load speeds $V = c_{min} = 22.5\,\mathrm{m\,s^{-1}}$(critical), $c_{min} < V = 40\,\mathrm{m\,s^{-1}} < \sqrt{gH}$(supercritical), $V = \sqrt{gH} = 58.6\,\mathrm{m\,s^{-2}}$ and $\sqrt{gH} < V = 70\,\mathrm{m\,s^{-2}}$. Figure 10 demonstrates how the viscoelasticity produces a small lag in the wave

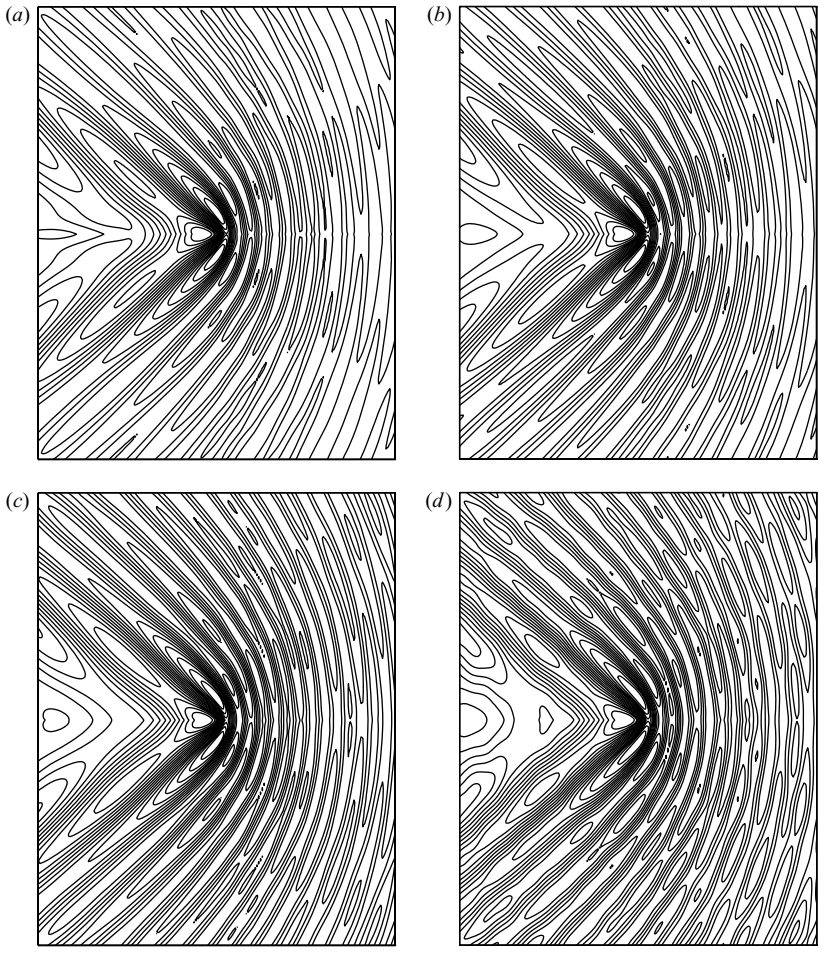

FIGURE 8. Time development of a two-dimensional wave pattern at a representative supercritical load speed. The parameters are $\alpha_0 = 0.1$; $A_0 = 0.01$; $V = 40\,\mathrm{m\,s^{-1}}$; $D = 7.324 \times 10^9$; $H = 350\,\mathrm{m}$; $g = 9.8\,\mathrm{m\,s^{-2}}$ and $\rho = 1000\,\mathrm{kg\,m^{-3}}$. (*a*) $t = 10\,\mathrm{s}$, (*b*) 30 s, (*c*) 60 s, (*d*) 100 s.

pattern, as was originally predicted in the steady-state theory of Hosking *et al.* (1988), with increasing effect as the viscoelastic parameter $A_0 \leqslant \alpha_0 = 0.1$ increases from zero.

Figure 11 illustrates the asymmetry of the profile of the ice deflection along the direction of motion of the load (when $y = 0$) at the subcritical load speed $V = 10\,\mathrm{m\,s^{-1}}$. Profiles for the elastic case and the anelastic case are shown at time $t = 5$, 25 and 100 s, for different values of the viscoelastic parameters A_0 and α_0. It can be seen that the asymmetry increases with increased viscoelasticity. The asymmetry in the elastic profile is due to time dependence and decreases with time.

Further attention was given to the time taken to approach a steady state, and also to the behaviour of the lag in the maximum depression behind the moving load (cf. Nugroho *et al.* 1999). Figure 12 shows profiles of the surface deflection at the times $t = 5$, 15, 25 and 35 s for the load speeds and parameters previously considered in figures 2 to 6 for the line load. The arrow marks the position of the load. Comparable profiles along the direction of motion of the load (when $y = 0$) are on the left, and

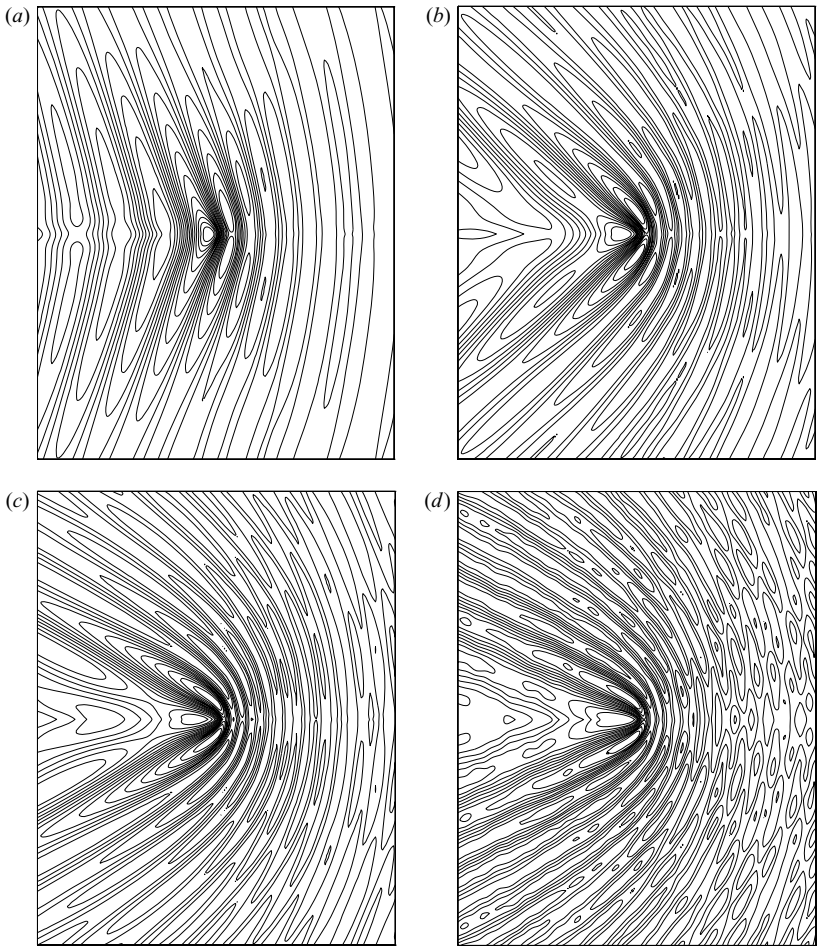

FIGURE 9. Contour of the developed two-dimensional wave pattern at critical, supercritical and higher load speeds. Other parameters are $\alpha_0 = 0.1$; $A_0 = 0.1$; $t = 10\,\mathrm{s}$; $D = 7.324 \times 10^9$; $H = 350\,\mathrm{m}$; $g = 9.8\,\mathrm{m\,s^{-2}}$ and $\rho = 1000\,\mathrm{kg\,m^{-3}}$. (*a*) $V = 22.5\,\mathrm{m\,s^{-1}}$, (*b*) $40\,\mathrm{m\,s^{-1}}$, (*c*) $58.6\,\mathrm{m\,s^{-1}}$, (*d*) $70\,\mathrm{m\,s^{-1}}$.

corresponding transverse profiles at the load (when $x = 0$) and also behind the load (at $x = 100$). It can be seen that the two-dimensional deflection approaches a steady state quite quickly, although it takes somewhat longer behind the load as expected. The profiles for the two load speeds $V = \sqrt{gH} = 58.6\,\mathrm{m\,s^{-1}}$ and $V = 70\,\mathrm{m\,s^{-1}}$ show the development of the shadow zone (cf. Davys *et al.* 1985). The increase of the lag in the maximum depression behind the load with time is also evident in the $y = 0$ profile.

Figure 13 shows more clearly how the lag (in metres) varies with time for load speeds V less than $\sqrt{gH}$. At first, while the deflection approaches its steady state, the lag is primarily due to time dependence. For the subcritical speed $V = 18\,\mathrm{m\,s^{-1}}$, the lag increases and then decays towards a small steady-state value. At the critical speed $V = c_{min} = 22.5\,\mathrm{m\,s^{-1}}$, the lag is constant after just a few seconds. For load speeds greater than the critical speed, the lag oscillates towards its steady value, at frequencies that increase with the load speed. (For load speeds greater than $\sqrt{gH}$, the shadow zone appears quickly, and the location of the lag is not well defined.)

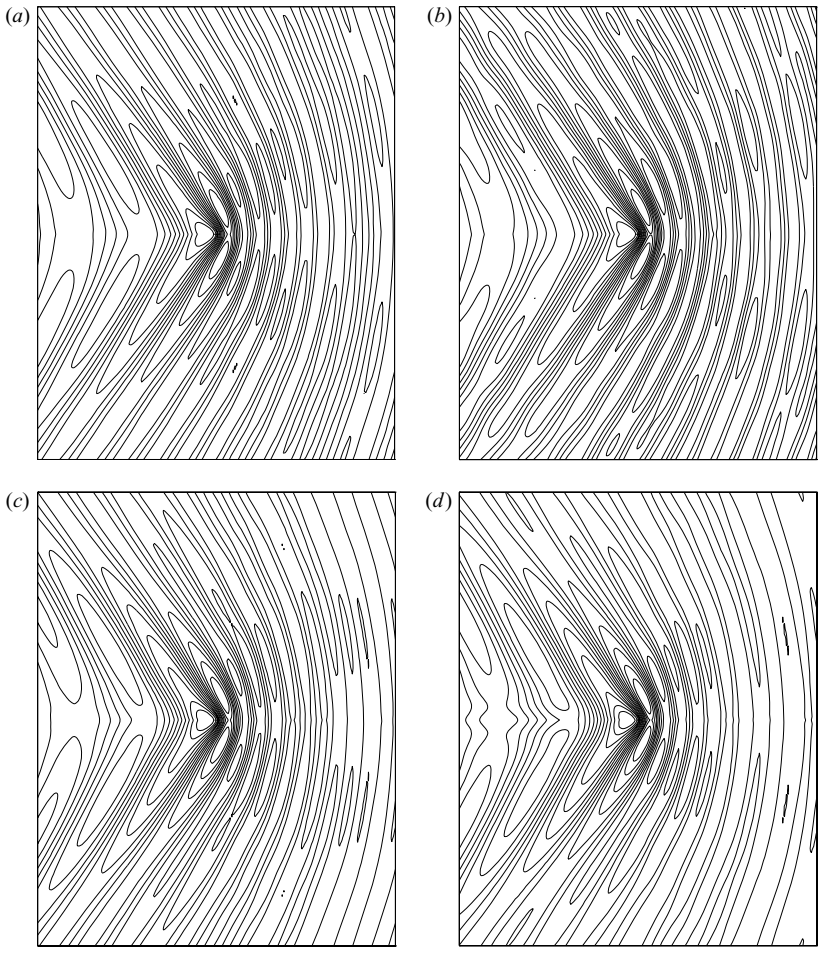

FIGURE 10. Contour of the developed two-dimensional wave pattern at supercritical load speed $V = 30\,\mathrm{m\,s^{-1}}$ for various viscoelastic parameters A_0. Other parameters are $\alpha_0 = 0.1$; $t = 10\,\mathrm{s}$; $D = 7.324 \times 10^9$; $H = 350\,\mathrm{m}$; $g = 9.8\,\mathrm{m\,s^{-2}}$ and $\rho = 1000\,\mathrm{kg\,m^{-3}}$. (*a*) $A_0 = 0$, (*b*) 0.01, (*c*) 0.05, (*d*) 0.1.

Figure 14 shows how the lag varies with time for different values of the viscoelastic parameters A_0 and α_0. Increasing A_0 increases the lag for all load speeds, but the lag depends much more weakly on the value of α_0. Viscoelasticity affects the lag relatively more at lower load speeds.

6. Discussion

Even if they travel for quite some time, moving loads usually produce ice sheet deflections small enough for linear theory to remain valid, but deflections observed in the vicinity of loads moving at or near the minimum phase speed c_{min} for the propagation of flexural–gravity waves are significantly larger. This phenomenon has been understood by noting that c_{min} coincides with the group speed of these flexural–gravity waves, so that the continual energy input from a load moving at speed c_{min} does not radiate away into the far field as it does at higher load speeds, but accumulates beneath the load in a solitary wave (subject to viscous dissipation).

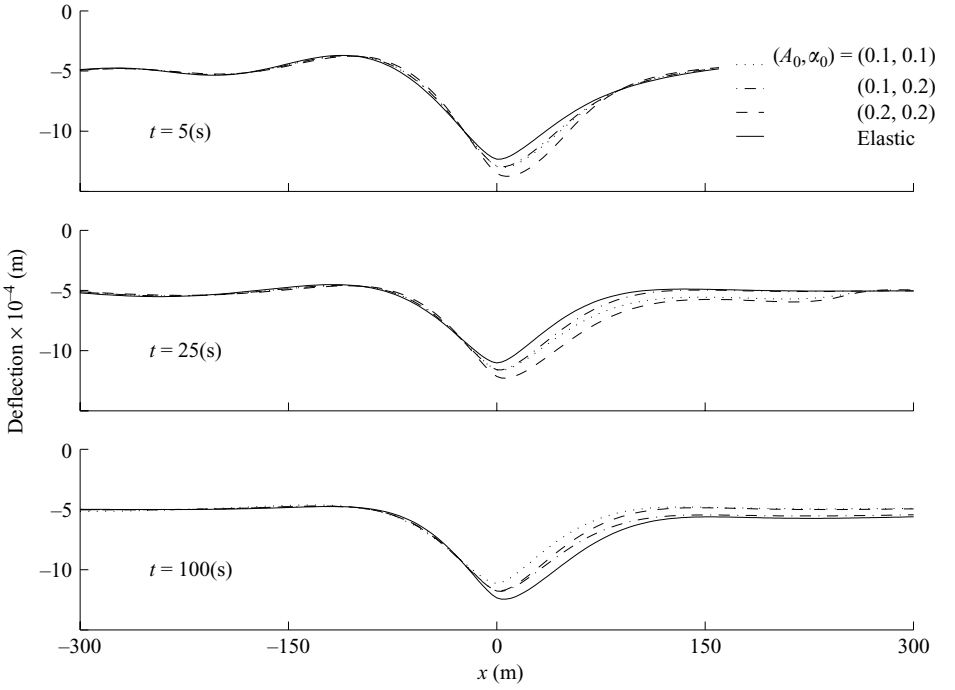

FIGURE 11. The centreline profile of the surface deflection along $y = 0$ for various viscoelastic parameters at different times. The parameters are $V = 10\,\mathrm{m\,s^{-1}}$; $D = 7.324 \times 10^9$; $H = 350\,\mathrm{m}$; $g = 9.8\,\mathrm{m\,s^{-2}}$ and $\rho = 1000\,\mathrm{kg\,m^{-3}}$.

Higher load speeds typically include the gravity wave speed $\sqrt{gH}$, which is, however, the lower bound for load speeds where 'shadow zones' appear, i.e. zones behind the moving load where no waves propagate, although wave energy radiates away elsewhere (cf. Davys *et al.* 1985; Squire *et al.* 1996).

As outlined in § 1, Kheysin (1971) and Schulkes & Sneyd (1988) discussed the one-dimensional time-dependent response of a floating elastic plate (i.e. to an instantaneously started line load). Their investigations were largely motivated by the unbounded deflection predicted for at least one particular load speed (subsequently identified with c_{min}) in the early time-independent theory of an elastic plate (Kheysin 1967; Nevel 1970), from the notion that such a response might be due to the load effectively acting upon the plate for an infinite time. However, Nevel had suggested that nonlinear effects, dissipation or ice inhomogeneity might remove the singularity he found for a distributed (circular) load. Indeed, time-independent theory for the one-dimensional and two-dimensional responses of a floating viscoelastic plate to a steadily moving load (i.e. to a line load and a point load, respectively) inter alia renders a pronounced but finite steady-state deflection at the critical speed c_{min} (Hosking *et al.* 1988). Further, more recent time-dependent theory for the response of a floating elastic plate to instantaneously started point and distributed (circular or rectangular) loads predicts that in two dimensions the response approaches a steady state at all other load speeds (whether subcritical or supercritical), including the gravity wave speed $\sqrt{gH}$ (Nugroho *et al.* 1999). The conclusion that a steady-state response is always produced in a floating plate by a steadily moving load (i.e. at all load speeds) is supported by the present time-dependent viscoelastic theory. Thus,

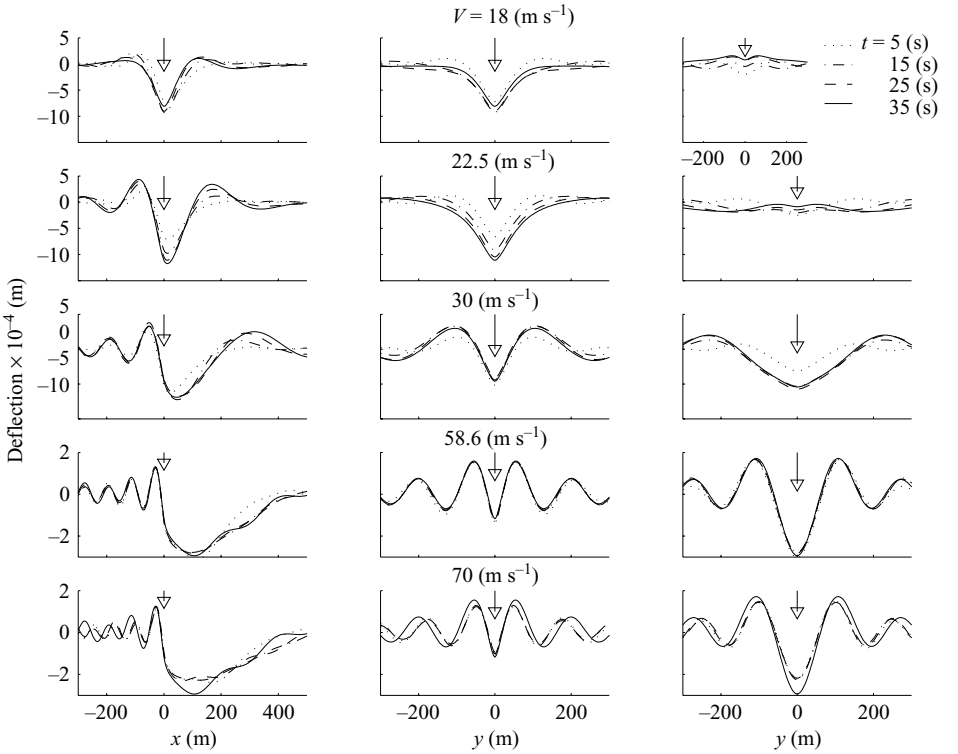

FIGURE 12. Profiles of the surface deflection along $y=0$, $x=0$, and $x=100\,(\mathrm{m})$ for different load speeds at different times. The parameters are $A_0=0.1=\alpha_0$; $D=7.324\times10^9$; $H=350\,\mathrm{m}$; $g=9.8\,\mathrm{m\,s^{-2}}$ and $\rho=1000\,\mathrm{kg\,m^{-3}}$.

the time-dependent anelastic deflections of a floating plate to an impulsively started moving line or point load limit (as time $t\to\infty$) to the results previously obtained by Hosking *et al.* (1988) for steadily moving loads, including the steady-state deflection at the critical load speed c_{min}.

The residual issue is therefore how quickly the steady state at any load speed is approached, and this question is also addressed in the present paper. For example, asymptotic analysis indicates that the associated transients at the critical speed c_{min} decay just as rapidly as do the transients at most higher load speeds. Indeed, in the preferred two-dimensional viscoelastic theory (for the anelastic deflections of a floating plate to an impulsively started moving point load) the transients present at the critical and higher load speeds generally decay more rapidly than their counterparts in the corresponding two-dimensional elastic theory (as t^{-2} rather than as t^{-1} for $t\to\infty$), except for a load travelling at the gravity wave speed $\sqrt{gH}$ when the elastic decay rate (as $t^{-1/3}$ for $t\to\infty$) prevails (cf. Nugroho *et al.* 1999). Numerical computations in the two-dimensional theory demonstrate that the viscoelastic deflection closely resembles its steady-state form in a matter of seconds after a load begins to move, and also illustrate the initial time dependence of the ultimately steady-state viscoelastic lag in the maximum deflection behind the load.

Parau & Dias (2002) considered nonlinear effects at load speeds approaching c_{min} from below in the thin elastic plate model, by including plate curvature in the plate equation and quadratic kinetic energy terms in the Bernoulli equation (cf. also Peake

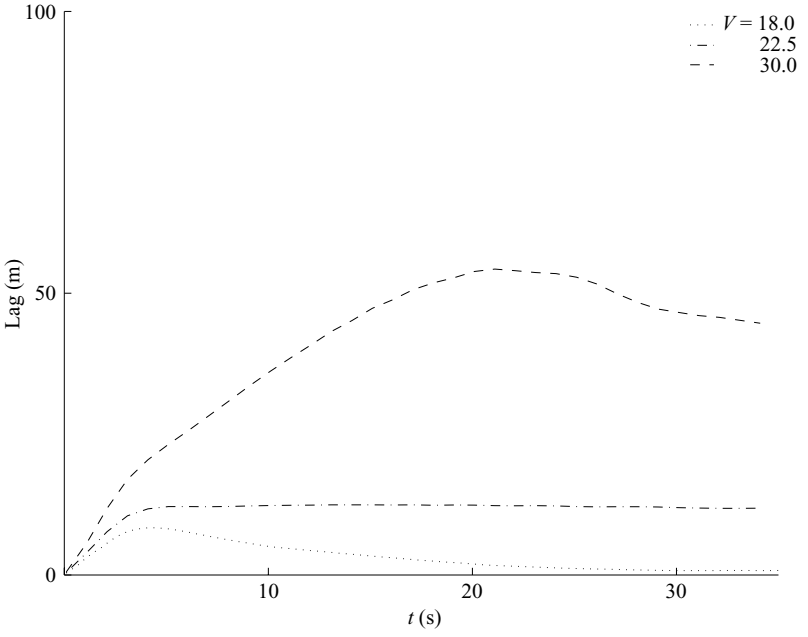

FIGURE 13. The lag, defined as the position of the maximum depression of the surface deflection as measured along the line $y = 0$, as a function of time at different load speeds. The parameters are $A_0 = 0.1 = \alpha_0$; $D = 7.324 \times 10^9$; $H = 350\,\mathrm{m}$; $g = 9.8\,\mathrm{m\,s^{-2}}$ and $\rho = 1000\,\mathrm{kg\,m^{-3}}$.

2001). More specifically, their contribution examines the steady deflections which may occur at load speeds less than or at c_{min}, albeit only for the one-dimensional case of a line load. They conclude that linear theory (which predicts a quasi-static response, similar to that due to a stationary load) is appropriate for load speeds not too close to c_{min}, and they find bounded deflections from their nonlinear theory for load speeds up to or approaching c_{min} (depending upon the water depth). Although the linearity assumption must break down if abnormally large deflections arise in the immediate vicinity of a load travelling at the critical speed c_{min}, the observational evidence is that a linear theory is otherwise appropriate for moving loads on ice sheets. However, since both viscoelasticity and nonlinearity separately produce a bounded response at c_{min}, a nonlinear viscoelastic theory might be developed to compare their relative and composite effect on the maximum deflection occurring at that speed.

K. W. was supported by an Overseas Postgraduate Research Scholarship, provided by the Commonwealth of Australia. R. J. H. is also grateful for financial support under the Research Grant UBD/PNC2/2/RG/1(29).

Appendix

Consider the cubic equation $\omega^3 + \mathrm{i}p\omega^2 + q\omega + \mathrm{i}r = 0$ where p, q and r are real. Substituting $\omega = x - \mathrm{i}p/3$ yields the 'reduced' Cardan form $x^3 + ax + b = 0$, where

$$a = \tfrac{1}{3}(3q + p^2), \qquad b = \frac{\mathrm{i}}{27}(-2p^3 - 9pq + 27r). \tag{A 1}$$

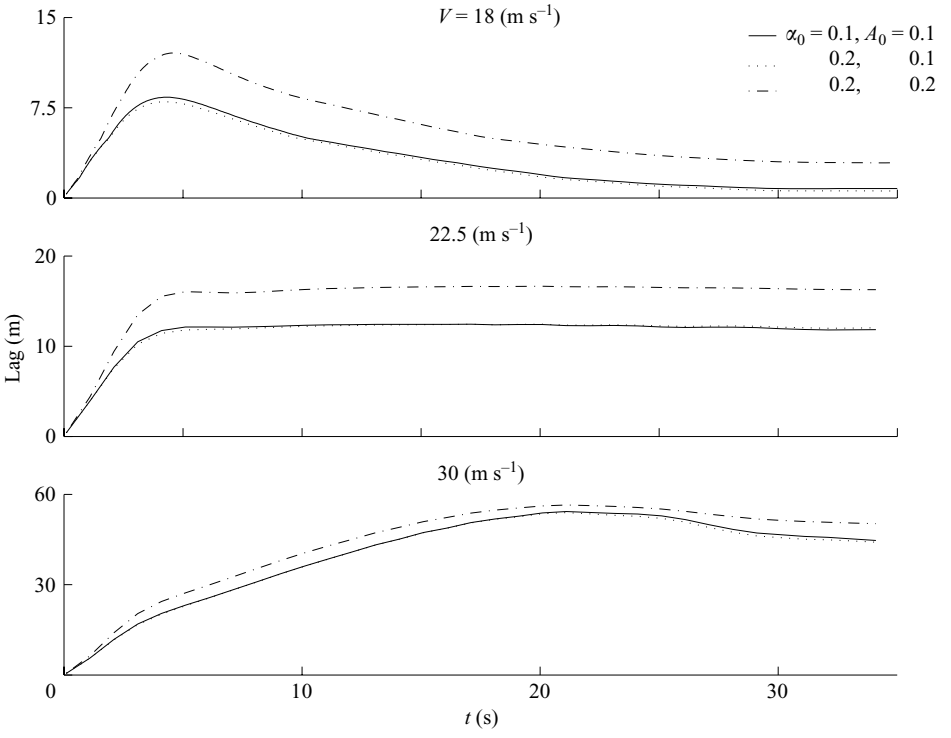

FIGURE 14. The lag, defined to be the position of the maximum depression of the surface deflection as measured along the line $y=0$, as a function of time at different load speeds and viscoelastic parameters. The parameters are $D=7.324\times10^9$; $H=350\,\mathrm{m}$; $g=9.8\,\mathrm{m\,s^{-2}}$ and $\rho=1000\,\mathrm{kg\,m^{-3}}$.

Note that a is real and b is pure imaginary, and the 'reduced' form has solution

$$x_1, x_2 = \pm\frac{\sqrt{3}}{2}(A-B) - \tfrac{1}{2}\mathrm{i}(A+B), \qquad x_3 = \mathrm{i}(A+B), \tag{A 2}$$

where

$$A = \sqrt[3]{-\frac{\mathrm{i}b}{2} + \sqrt{-\left(\frac{a^3}{27}+\frac{b^2}{4}\right)}}, \qquad B = \sqrt[3]{-\frac{\mathrm{i}b}{2} - \sqrt{-\left(\frac{a^3}{27}+\frac{b^2}{4}\right)}}. \tag{A 3}$$

Since $a^3/27 + b^2/4$ is real and negative for p, q, r defined in (7) when $k\neq0$, both A and B are real even functions in k ($A>B$), defining two complex roots and one pure imaginary root in (A 2) and consequently $\omega_{1,2}$ and ω_3 in (8) in the main text. There are several relevant results, summarized as follows.

THEOREM

(i) $\mathrm{Im}(\omega_{1,2})>0$ (*for* $k\neq0$);

(ii) $\mathrm{Im}(\omega_3)>0$;

(iii) $A+B$ *is monotonically increasing on* $(-\infty,0)$, *and monotonically decreasing on* $(0,\infty)$;

(iv) *In the neighbourhood of* $k=0$,

$$\omega_{1,2} = \pm\sqrt{gH}|k|(1-k^2H^2/6+\cdots) + \mathrm{i}O(k^6),$$
$$\omega_3 = \mathrm{i}[\alpha_0 - O(k^6)].$$

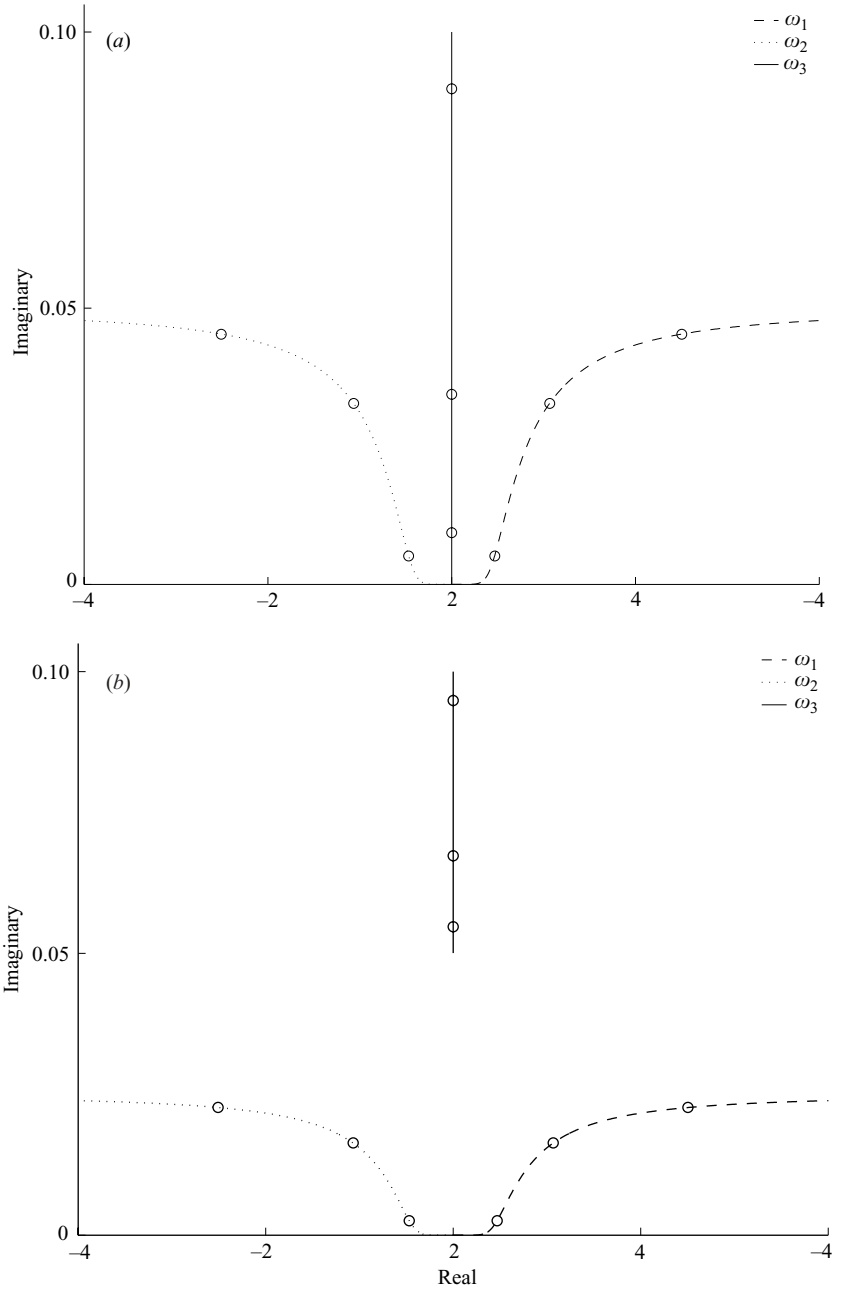

FIGURE 15. The contours of the three roots in the complex plane near $k = 0$. The circles correspond to the values $k = 0.02$, 0.04 and 0.06 with the imaginary part of each root increasing with k. (*a*) $A_0 = 0.1$, (*b*) $A_0 = 0.05$. The other parameters are $\alpha_0 = 0.1$, $D = 7.324 \times 10^9$; $H = 350\,\mathrm{m}$; $g = 9.8\,\mathrm{m\,s^{-2}}$ and $\rho = 1000\,\mathrm{kg\,m^{-3}}$.

Proof. Since the roots $\omega_{1,2,3}$ defined by the real even functions A and B (and viscoelastic constant α_0) are even in k, let us restrict our attention to the domain $0 < k < \infty$.

(i) Using $(A+B)^3 = A^3+B^3+3AB(A+B)$ and $AB = a/3$, it follows that $\mathrm{Im}(\omega_{1,2}) = 0$ is equivalent to $-\mathrm{i}b - 2ap/3 = -8p^3/27$, or $pq = r$. For p, q, r defined in (8) that is $k\tanh(kH)Dk^4A_0/\rho = 0$, which is satisfied if and only if $k = 0$. For any arbitrary $k \neq 0$, one finds $\mathrm{Im}(\omega_{1,2}) > 0$.

(ii) If $\mathrm{Im}(\omega_3) = 0$ for some k, again using $(A+B)^3 = A^3 + B^3 + 3AB(A+B)$ and $AB = a/3$ one has $-\mathrm{i}b + ap/3 = p^3/27$ implying $r = 0$ or $k\tanh(kH)[(Dk^4 + pg)\alpha_0 - Dk^4A_0] = 0$ from (8), and hence $k = 0$ since $A_0 \leqslant \alpha_0$. But when $k \to 0$, both q and r tend to zero and $\mathrm{Im}(\omega_3)$ approaches its maximum $\alpha_0 > 0$, therefore ω_3 has no zero and $\mathrm{Im}(\omega_3) > 0$.

(iii) Writing $C = A + B$ for convenience, one has that $C^3 = -\mathrm{i}b + aC$ and consequently $(3C^2 - a)C' = -\mathrm{i}b' + a'C$, where the prime denotes differentiation with respect to k. Now $3C^2 - a = 3(C^2 - AB) = 3(A^2 + AB + B^2) > 0$, since $a = 3AB$ and the quadratic form $\lambda^2 + \lambda + 1$ (with $\lambda \equiv A/B > 0$) is positive definite. On the other hand, $C \leqslant 2\alpha_0/3 = -2p/3$ so that $-\mathrm{i}b' + a'C = -pq'/3 + r' + q'C \leqslant -pq'/3 + r' - 2pq'/3 = -pq' + r' \leqslant 0$, since $-pq + r = -A_0Dk^5\tanh(kH)/\rho$ monotonically decreases as k increases. Hence $C' \leqslant 0$, so that $C = A + B$ monotonically decreases from its maximum value $2\alpha_0/3$ at $k = 0$ ($C' = 0$ only occurs at $k = 0$).

(iv) The results follow by straightforward calculation, or by using some symbolic computational tool (e.g. MATLAB).

Figure 15(a) shows the contours of the three roots in the complex plane for $A_0 = \alpha_0 = 0.1$. The circles correspond to the values $k = 0.02$, 0.04 and 0.06. It can be seen that the difference between the elastic and the anelastic case is near $k = 0$ where $\omega_3 \neq 0$, and for large k where $\mathrm{Im}(\omega_1) = \mathrm{Im}(\omega_2) \neq 0$. For comparison, figure 15(b) shows the corresponding results for $A_0 = 0.05$ and $\alpha_0 = 0.1$, where ω_3 does not tend to zero as k goes to infinity.

REFERENCES

Bukatov, A. E. & Zharkov, V. V. 1989 Three-dimensional bending gravitational oscillations near moving pressure regions. *J. Appl. Mech. Tech. Phys.* **30**, 490–497.

Davys, J. W., Hosking, R. J. & Sneyd, A. D. 1985 Waves due to a steadily moving source on a floating ice plate. *J. Fluid Mech.* **158**, 269–287.

Hosking, R. J., Sneyd, A. D. & Waugh, D. W. 1988 Viscoelastic response of a floating ice plate to a steadily moving load. *J. Fluid Mech.* **196**, 409–430.

Kheysin, D. Ye. 1963 Moving load on an elastic plate which floats on the surface of an ideal fluid. *Izv. Akad. Nauk SSSR, Otd. Tekh. Nauk, Mekh. i Mashinostroenie* **1**, 178–180 (in Russian).

Kheysin, D. Ye. 1967 Dynamics of floating ice covers (in Russian). *Gidrometeorologichoskoe Izdatel'stvo, Leningrad, 1967*, Technical Translation FSTC-HT-23-485-69, U.S. Army Foreign Science and Technology Center (in Russian).

Kheysin, D. Ye. 1971 Some non-stationary problems of dynamics of the ice cover. In *Studies in Ice Physics and Ice Engineering* (ed. G. N. Yakovlev), pp. 81–91. Israel Program for Scientific Translations.

Milinazzo, F., Shinbrot, M. & Evans, N. W. 1995 A mathematical analysis of the steady response of floating ice to the uniform motion of a rectangular load. *J. Fluid Mech.* **287**, 173–197.

Nevel, D. E. 1970 Moving loads on a floating ice sheet. *CRREL Res. Rep.* 261. Cold Regions Research and Engineering Laboratory, Hanover, New Hampshire, USA.

Nugroho, W. S., Wang, K., Hosking, R. J. & Milinazzo, F. 1999 Time-dependent response of a floating flexible plate to an impulsively started steadily moving load. *J. Fluid Mech.* **381**, 337–355.

Olver, F. W. J. 1974 *Introduction to Asymptotics and Special Functions.* Academic.

Parau, E. & Dias, F. 2002 Nonlinear effects in the response of a floating ice plate to a moving load. *J. Fluid Mech.* **460**, 281–305.

Peake, N. 2001 Nonlinear stability of a fluid-loaded elastic plate with mean flow. *J. Fluid Mech.* **434**, 101–118.

Schulkes, R. M. S. M. & Sneyd, A. D. 1988 Time-dependent response of floating ice to a steadily moving load. *J. Fluid Mech.* **186**, 25–46.

Squire, V. A., Hosking, R. J., Kerr, A. D. & Langhorne, P. J. 1996 *Moving Loads on Ice Plates.* Kluwer.

Wong, R. 1989 *Asymptotic Approximations of Integrals.* Academic.